Available online at www.sciencedirect.com
ScienceDirect
International Journal of Pharmaceutics 346 (2008) 133–142
INTERNATIONAL JOURNAL OF PHARMACEUTICS
www.elsevier.com/locate/ijpharm

Pharmaceutical Nanotechnology

Preparation and characterization of thermo-responsive albumin nanospheres

Zhe-Yu Shen [a,b,c], Guang-Hui Ma [a,*], Toshiaki Dobashi [b], Yasuyuki Maki [b], Zhi-Guo Su [a]

[a] *State Key Laboratory of Biochemical Engineering, Institute of Process Engineering, Chinese Academy of Sciences, P.O. Box 353, Beijing 100080, China*
[b] *Department of Biological and Chemical Engineering, Faculty of Engineering, Gunma University, 1-5-1, Tenjin-cho, Kiryu, Gunma 376-8515, Japan*
[c] *Graduate University of Chinese Academy of Sciences, 19, Yuquan Road, Shijingshan District, Beijing 100049, China*

Received 18 January 2007; received in revised form 9 April 2007; accepted 6 June 2007
Available online 14 June 2007

Abstract

Thermo-responsive poly(*N*-isopropylacrylamide-*co*-acrylamide)-*block*-polyallylamine-conjugated albumin nanospheres (PAN), new thermal targeting anti-cancer drug carrier, was developed by conjugating poly(*N*-isopropylacrylamide-*co*-acrylamide)-*block*-polyallylamine (PNIPAM-AAm-*b*-PAA) on the surface of albumin nanospheres (AN). PAN may selectively accumulate onto solid tumors that are maintained above physiological temperature due to local hyperthermia. PNIPAM-AAm-*b*-PAA was synthesized by radical polymerization, and AN was prepared by ultrasonic emulsification. AN with diameter below 200 nm and narrow size distribution was obtained by optimizing the preparative conditions. Rose Bengal (RB) was used as model drug for entrapment into the AN and PAN during the particle preparation. The release rate of RB from PAN compared with AN in trypsin solution was slower, and decreased with the increase of PNIPAM-AAm-*b*-PAA molecular weight, which suggested that the existence of a steric hydrophilic barrier on AN made digestion of AN more difficult. Moreover, the release of RB from PAN above the cloud-point temperature (T_{cp}) of PNIPAM-AAm-*b*-PAA became faster. This was because the density of temperature-responsive polymers on AN was not so high, so that the interspace between the polymer chains increased after they shrunk due to the high temperature. As a result, the biodegradable AN was attacked more easily by trypsin. The design of PAN overcame the disadvantages of temperature-responsive polymeric micelles.

Keywords: Poly(*N*-isopropylacrylamide-*co*-acrylamide)-*block*-polyallylamine; Albumin nanospheres; Rose Bengal; Entrapment efficiency; Controlled release

1. Introduction

The main problems currently associated with systemic drug administration are: even biodistribution of pharmaceuticals throughout the body; lack of drug specific affinity toward a pathological site; the necessity of a large total dose of drug to achieve high local concentration; non-specific toxicity and other adverse side-effects due to high drug doses. Because of these drawbacks of systemic drug administration and the toxicity of anti-cancer drugs to both tumor and normal cells, the efficacy of cancerous chemotherapy is often limited by serious side-effect. A strategy could be to associate anti-cancer drugs with colloidal nanoparticles, with the aim to increase selectivity of drugs towards cancer cells while reducing their toxicity towards normal tissues (Brigger et al., 2002). The accumulation of intravenously injected nanoparticles onto tumor cells relies on a passive diffusion or convection across the leaky and hyperpermeable tumor vasculature (Yuan, 1998), which was called passive targeting. Indeed, the uptake of nanoparticles can also result from active targeting, a specific recognition in the case of ligand decorated nanoparticles (Moghimi et al., 2001). To date, many distinctive active targeting nanoparticles, such as folate-conjugated albumin nanoparticles (Zhang et al., 2004), monoclonal antibody conjugated nanoparticles (Sheng et al., 1995), magnetic albumin nanoparticles (Gong et al., 2004), pH- and temperature-responsive polymeric micelles (Kwon et al., 1995; Topp et al., 1997; Inoue et al., 1998; Chung et al., 2000; Jeong et al., 2003), have been investigated in drug delivery applications.

The temperature-responsive polymeric micelles were constructed by hydrophobic interaction, which is weak comparing with covalent bond. When it arrived at the heated cancer tissues

* Corresponding author. Tel.: +86 1082627072; fax: +86 1082627072.
E-mail address: ghma@home.ipe.ac.cn (G.-H. Ma).

0378-5173/$ – see front matter © 2007 Elsevier B.V. All rights reserved.
doi:10.1016/j.ijpharm.2007.06.004

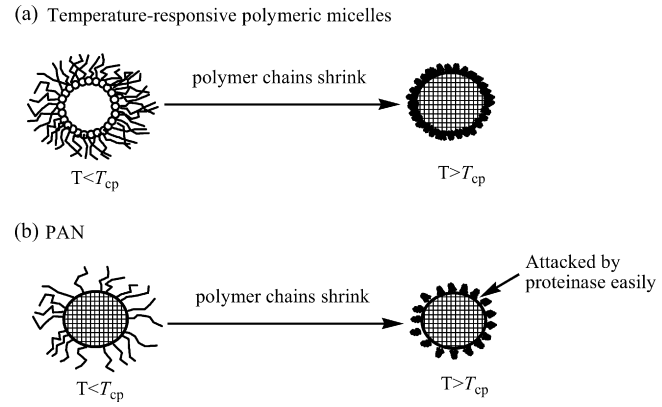

Scheme 1. Schematic presentation for difference of (a) temperature-responsive polymeric micelles and (b) PAN.

and cells, it could accumulate on the cancer tissues and cells (Kohori et al., 1999). However, the dense hydrophilic polymer sequence on the surface of temperature-responsive polymeric micelles would shrink and accumulate on the micelles (as shown in Scheme 1a), resulting in the decrease of the drug release rate from the micelles and the curative efficacy.

In this study, we developed a new thermal targeting anti-cancer drug carrier: temperature-responsive polymer conjugated albumin nanospheres. At first, biodegradable albumin nanospheres (AN) with Rose Bengal (RB, model drug) inside was prepared by ultrasonic emulsification combined with chemical cross-linking (glutaraldehyde), then poly(*N*-isopropylacrylamide-*co*-acrylamide)-*block*-allylamine (PNIPAM-AAm-*b*-PAA) (thermo-responsive polymers) was conjugated on AN. This PNIPAM-AAm-*b*-PAA-conjugated albumin nanospheres (PAN) was designed by following strategy.

On intravenous administration, particles are normally rapidly coated by the adsorption of specific blood components known as opsonins and then recognized and taken up by the reticuloendothelial system (RES). The surface of albumin nanospheres with drug inside and thermo-responsive copolymer chains on the surface is hydrophilic at and below 37 °C due to the hydrophilicity of the copolymer if the cloud-point temperature (T_{cp}) of the copolymer is about 42 °C under local hyperthermia. This hydrophilic copolymer layer can dramatically affect the opsonization of particles by plasma components (Moghimi et al., 1993; Lin et al., 1999). Therefore, the uptake of PAN by the RES can be reduced and a significantly longer circulation half-life of the particles in the blood stream will be obtained (Illum and Davis, 1984). PAN will not precipitate on the healthy tissues and cells because of the hydrophilic surface, but will precipitate on the heated cancer tissues and cells around 42 °C, because the copolymer will become hydrophobic at higher temperature due to conformational transition of the chain. Then, the interspace between the temperature-responsive polymer chains (as shown in Scheme 1b) will increase after they shrink due to the high temperature. So that, the biodegradable albumin nanospheres will be attacked and degraded more easily by proteinase, then the drug will release there to attack the tumor cells. Furthermore, histological analysis of PNIPAM-grafted gelatin gel elucidated that PNIPAM can be biodegraded over time without excessive inflammatory reactions (Ohya et al., 2004). According to a toxicity test of the PNIPAM, which was performed in comparison with that of the NIPAM monomer, PNIPAM showed no toxicity in mice (Sheng et al., 2006). Therefore, although NIPAM, AAm and AA are toxic monomers, PNIPAM-AAm-*b*-PAA is also biodegradable over time and non-toxic.

Consequently, PAN, which is constructed by covalent bond and whose drug release above T_{cp} of PNIPAM-AAm-*b*-PAA is faster, can be employed as drug carrier due to their targeting ability to tumor cells by both passive and active targeting.

2. Materials and methods

2.1. Materials

N-isopropylacrylamide (NIPAM), 2,2′-azobis(isobutyronitrile) (AIBN) and Rose Bengal (RB) were purchased from Tokyo Chemical Industry Co., Ltd. (TCI, Japan). NIPAM was purified by recrystallization from *n*-hexane. Acry-

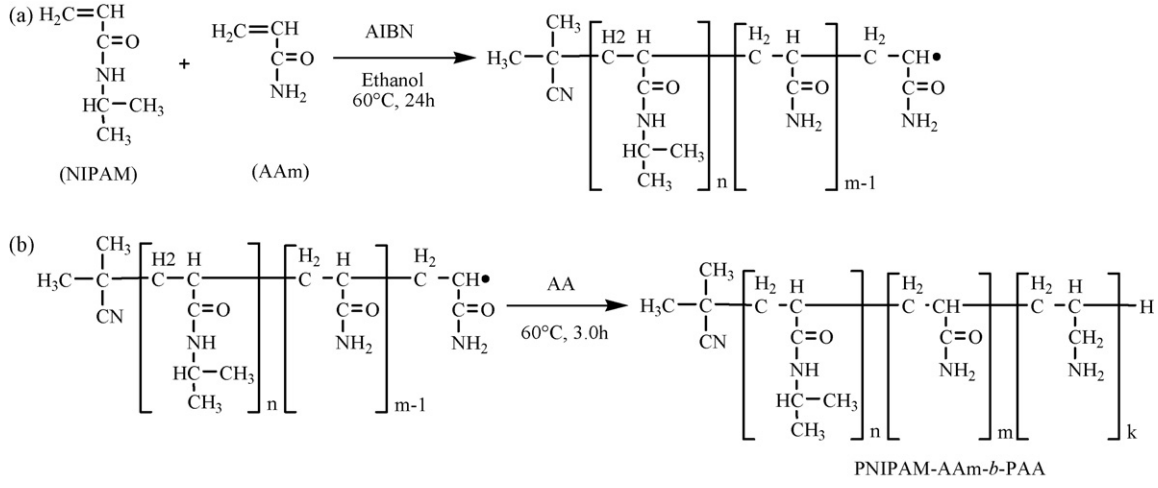

Scheme 2. Reaction scheme for PNIPAM-AAm-*b*-PAA.

lamide (AAm) and sorbitan sesquioleate (Arlacel83) were purchased from SIGMA (USA). Allylamine (AA), 50% glutaraldehyde (GA) aqueous solution, trypsin (30 USP units/mg), *N*-hydroxysuccinimide (NHS) and 1-ethyl-3-(3-dimethylaminopropyl) carbodiimide (EDAC) were purchased from Wako Pure Chemicals (Tokyo, Japan). Bovine serum albumin (BSA), fraction V (pH 7.0), was purchased from ICN Biomaterials.

2.2. Synthesis of thermo-sensitive polymers

Poly(*N*-isopropylacrylamide-*co*-acrylamide)-*block*-polyallylamine (PNIPAM-AAm-*b*-PAA) was synthesized from two steps (Scheme 2) by free radical polymerization using AIBN as an initiator. First, 39.05 g of NIPAM, 2.95 g of AAm, AIBN and 250 mL of ethanol were added into a three-necked round-bottle flask with a magnetic stirrer. The round-bottle flask was moved in an oil bath and stirred at 60 °C for 24 h under nitrogen atmosphere. Second, after 24 h, 2 mL of AA was dropwise added into the mixture. The whole mixture was stirred at 60 °C for 3.0 h under nitrogen atmosphere. 0.20 and 0.10 g of AIBN were used to obtain PNIPAM-AAm-*b*-PAA1 and PNIPAM-AAm-*b*-PAA2, respectively. The resultant polymers were separated and purified by reprecipitation into diethylether and then dried in vacuum. The polymers were dissolved in MilliQ water for optical transmittance measurement. Gel permeation chromatography (GPC) measurements were made on PNIPAM-AAm-*b*-PAA1 and PNIPAM-AAm-*b*-PAA2 in THF at 35 °C using a Waters GPC equipment (Waters 515 HPLC Pump, Waters Styragel Columns [HT2 + HT3 + HT4], Waters 2410 Differential Refractometer). The flow rate and the temperature of the column oven were set to be 1 $cm^3\ min^{-1}$ and 35 °C, respectively. Elution times were converted into molecular weights using a calibration curve constructed with narrow polydispersity polystyrene standards, whose molecular weights range from 2500 to 600,000.

2.3. Preparation of blank and RB-loaded albumin nanospheres

Albumin nanospheres were prepared by an ultrasonic emulsification method combined with chemical cross-linking. The preparation method is as follows.

0.6 mL of 20% BSA physiological saline was added into 30 mL cyclohexane containing 6.0 wt.% of Arlacel83 and stirred for 10 min. Then, the solution was emulsified for 10 min by ultrasonic disruptor (TOMY UD-200) with the output power of 71, 97, 127 and 165 W, respectively. After that, glutaraldehyde toluene solution (0.85 mg GA/mg BSA) was added to cross-link the particles. The cross-linking process was performed by stirring the suspension over 24 h. 0.5 mL of 2-aminoethanol was then added to cap free aldehyde groups (Scheme 3a). After a 1.0 h reaction time, the suspension was ultracentrifuged (44,900 × *g*, 20 min) at 10 °C (Automatic Preparative Ultracentrifuge, HITACHI 70P-72, Japan). The harvested nanospheres were washed two times by cyclohexane to remove the emulsifier and then acetone was dropwise added into 20 mL of AN cyclohexane solution under stirring until the solution became just turbid. After ultracentrifuged, the samples were dried in vacuum for 1.0 h. And then, the nanospheres were cleaned one time by pure water to eliminate free albumin and the excess of the cross-linker. Between each washing, nanospheres were

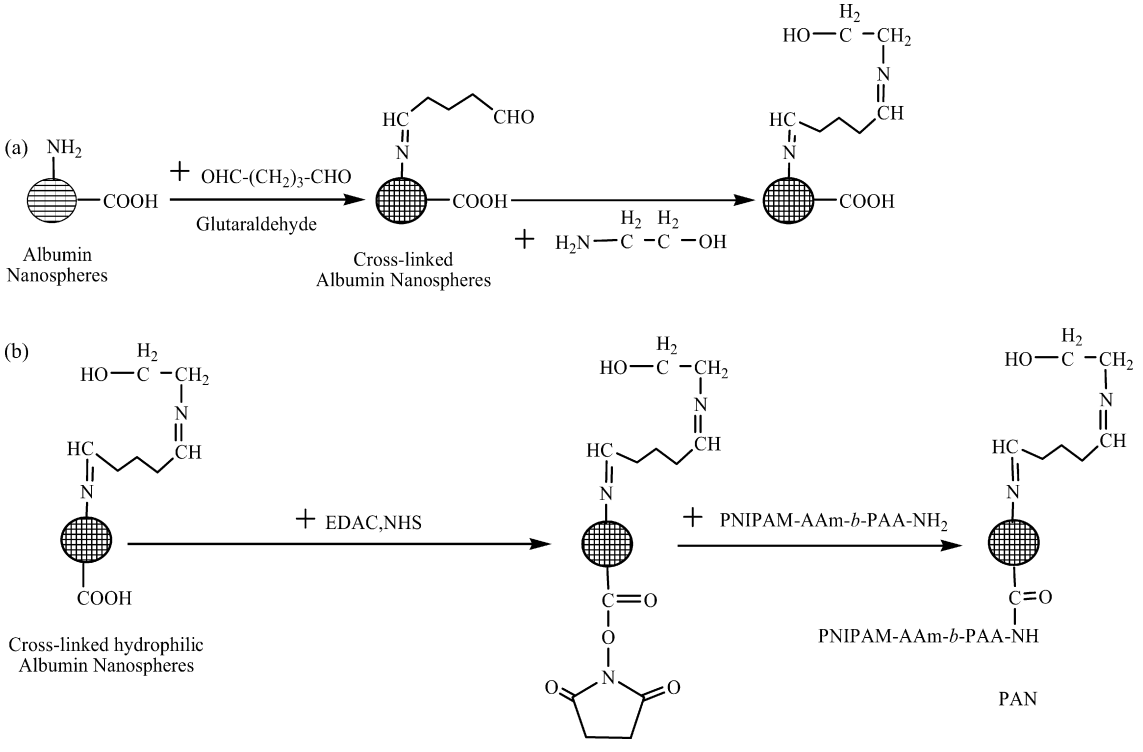

Scheme 3. Reaction scheme for preparation of cross-linked AN and conjugation of PNIPAM-AAm-*b*-PAA on AN.

Table 1
DLS results of blank AN

Sample	Output power[a] (W)	Mean diameter[b] (nm)	CV	Yield[c] (%)
AN1	71	169	0.26	83
AN2	97	149	0.16	80
AN3	127	134	0.14	88
AN4	165	102	0.14	82

[a] The output power of the ultrasonic disruptor for preparing AN.
[b] Determined by DLS in pure water at room temperature.
[c] Calculated from the weight ratio of AN to feed weight of BSA.

ultracentrifuged and supernatants were discarded. After that, the albumin nanospheres were lyophilized for 48 h. The results are summarized in Table 1.

RB-loaded albumin nanospheres (RB-AN) were prepared by the same method. RB-AN1, RB-AN2, RB-AN3 and RB-AN4 were prepared with a variable amount of RB (ranging from 0.63 to 5.00 μg/mg BSA) dissolved in 20% BSA physiological saline. RB-AN5, RB-AN6 and RB-AN7 were prepared at 8.0, 4.0 and 2.0 wt.% of Arlacel83, respectively. RB-AN8, RB-AN9, RB-AN10 and RB-AN11 were prepared with a variable amount of glutaraldehyde (ranging from 0.28 to 1.98 mg GA/mg BSA). The preparative conditions and the results of these samples are summarized in Table 2.

2.4. Preparation of PNIPAM-AAm-b-PAA-conjugated albumin nanospheres

After cleaned by pure water, the harvested AN4 sample was dispersed in 10 mL of phosphate buffer (pH 4.0, 100 mM). 0.25 g of EDAC and 0.30 g of NHS were dissolved in 10 mL of cold phosphate buffer, and then the buffer was dropwise added into the AN suspension. EDAC activation was done for 2.0 h at room temperature. The unreacted EDAC and NHS were removed by ultracentrifugation and the AN were resuspended in 10 mL of phosphate buffer. 5.0 mL of PNIPAM-AAm-*b*-PAA solution (0.10 g/mL) was added into the suspension and the mixture was stirred at room temperature for 3.0 h (Scheme 3b). After that, PNIPAM-AAm-*b*-PAA-conjugated AN (PAN) was ultracentrifuged to remove unreacted PNIPAM-AAm-*b*-PAA (the supernatant was transferred to a new tube for further analysis), then were lyophilized and stored at −20 °C. PNIPAM-AAm-*b*-PAA1 and PNIPAM-AAm-*b*-PAA2 were used to prepare PAN1 and PAN2, respectively. The unreacted PNIPAM-AAm-*b*-PAA1 and PNIPAM-AAm-*b*-PAA2 in the supernatant were quantified by conductometric titration with 2.0×10^{-3} M HCl. So that, the amounts of PNIPAM-AAm-*b*-PAA1 and PNIPAM-AAm-*b*-PAA2 on the surface of AN can be calculated.

RB-loaded PAN1 (RB-PAN1) and RB-loaded PAN2 (RB-PAN2) were prepared by the same method, but 2.5 μg RB/mg BSA was dissolved in 20 wt.% BSA physiological saline before emulsification by ultrasonic disruptor.

2.5. Optical transmittance and dynamic light scattering measurement

Optical transmittance (OT) of aqueous polymer solutions (5.00 mg/mL) was measured from lower to higher temperatures at 500 nm of wavelength with a visible optical spectrophotometer (HITACHI, U-2000 Spectrophotometer). A sample cell with a path length of 10 mm was used. Heating rate was 0.1 °C/min. The cloud-point temperature (T_{cp}) of a polymer solution was determined at a temperature showing an optical transmittance of 50%.

Particle size and size distribution of AN1, AN2, AN3 and AN4 (before washed by pure water) were measured by dynamic light scattering (DLS) at the scattering angle of 90° in anhydrous cyclohexane at room temperatures using a laboratory-made light scattering apparatus (Isojima et al., 1999) with a BI-9000AT correlator (Brookhaven). Vertically polarized incident light of 532 nm wavelength (a diode laser, BWT-50, B&W) was used. AN solutions were optically cleaned through a 0.45 μm membrane filter just before measurements. The number-average diameter ($\bar{d}$) and size distribution (CV, coefficient of variation)

Table 2
Preparative conditions and results of RB-AN

Sample	RB/BSA ratio (μg/mg)	$C_{Arlacel83}$ (wt.%)	GA/BSA ratio (mg/mg)	Yield[a] (%)	Drug loading ratio[b] (μg RB/mg AN)	Entrapment efficiency[b] (%)
RB-AN1	5.00	6.0	0.85	95.8	2.05	42.0
RB-AN2	2.50	6.0	0.85	91.3	1.88	73.3
RB-AN3	1.25	6.0	0.85	88.3	1.06	79.8
RB-AN4	0.63	6.0	0.85	85.2	0.57	83.0
RB-AN5	2.50	8.0	0.85	89.8	1.85	70.9
RB-AN6	2.50	4.0	0.85	87.4	1.91	71.4
RB-AN7	2.50	2.0	0.85	85.9	1.74	63.7
RB-AN8	2.50	6.0	1.98	96.8	1.87	77.4
RB-AN9	2.50	6.0	1.42	89.0	1.99	75.7
RB-AN10	2.50	6.0	0.85	90.5	1.96	75.6
RB-AN11	2.50	6.0	0.28	86.6	1.07	39.7
RB-PAN1	2.50	6.0	0.85	–	1.08	39.3
RB-PAN2	2.50	6.0	0.85	–	0.91	36.1

[a] Calculated from the weight ratio of AN to feed weight of BSA and drug.
[b] Determined by UV spectrophotometer and calculated from the standard calibration curve.

were defined as follows:

$$\bar{d} = \sum_{i=1}^{n} \frac{d_i}{N}$$

$$CV = \left(\sum_{i=1}^{n} \frac{(d_i - \bar{d})^2}{N} \right)^{1/2} / \bar{d}$$

where d_i is the diameter of each particle, N the total number of measured particles and $\bar{d}$ is the number-average diameter.

PAN1 and PAN2 were also measured by DLS from lower to higher temperatures in pure water. The solutions were equilibrated at given temperatures for 10 min before each measurement. Diffusion coefficient was obtained by cumulant method and the hydrodynamic diameter (D_h) was estimated from the diffusion coefficient by using the Stokes–Einstein equation.

2.6. Transmission electron microscopic observation

The AN4 and PAN1 were observed by a JEM-100cx (JEOL, Japan) transmission electron microscope (TEM). Approximately 2 μL of the diluted nanoparticles were mounted on copper grids, and then dried at room temperature. After that, they were observed by TEM (no coloration).

2.7. Determination of drug loading ratio and entrapment efficiency

The RB content was measured by digesting 24 mg of RB-AN (or RB-PAN) and corresponding blank-AN (or blank-PAN) in 6 mL of 20 mg/mL trypsin solution in the dark for 4.0 h at 37 °C, respectively. The digested solutions of blank-AN and blank-PAN were used to make baseline of absorbance measurement by UV spectrophotometer (HITACHI, U-2000 Spectrophotometer). The absorbance (at 548 nm of wavelength) of the digested solutions of RB-AN (or RB-PAN) was converted into the concentration of RB using a calibration curve constructed with standard RB solutions containing 4.0 mg/mL BSA and 20 mg/mL trypsin. The drug loading ratio (DLR, μg RB/mg AN) and entrapment efficiency (EE%) were calculated from the following formula:

$$DLR = \frac{\text{Total amount of RB loaded (μg)}}{\text{Total amount of nanospheres harvested (mg)}} \quad (1)$$

$$EE(\%) = \frac{\text{Total amount of RB loaded}}{\text{Total amount of RB added}} \times 100 \quad (2)$$

2.8. 'In vitro' release studies

Thirty milligrams RB-AN (or RB-PAN) were dispersed in 20 mL of phosphate-buffered saline (PBS, pH 7.4, 10 mM) with or without 0.20 mg/mL of trypsin. The suspensions were stirred slowly and incubated in a water bath at 37 ± 1 °C. At predetermined time intervals, these samples were ultracentrifuged at 44,900 × g for 20 min and 1.0 mL of these supernatants were taken and analyzed for concentration of the released RB by spectrophotometer. The release of RB from RB-AN9 and RB-AN10 without trypsin, and from RB-AN8, RB-AN9, RB-AN10 and RB-AN11 with 0.20 mg/mL of trypsin were determined. Moreover, the release of RB from RB-PAN1 and RB-PAN2 with 0.20 mg/mL of trypsin was both determined at 37 ± 1 °C and 43 ± 1 °C.

RB of RB-AN10 was released for 8.0 h in PBS with 0.20 mg/mL of trypsin at 37 ± 1 °C. Then RB-AN10 was recovered and renamed as RB-AN12. The release of RB from RB-AN12 with 0.20 mg/mL of trypsin was determined at 37 ± 1 °C.

3. Results and discussion

3.1. Polymerization results

The yield determined as diethylether insoluble fraction for PNIPAM-AAm-*b*-PAA1 and PNIPAM-AAm-*b*-PAA2 was 74 and 78%, respectively. The molecular weights M_w determined from GPC were 1.43×10^4 and 1.59×10^4 for PNIPAM-AAm-*b*-PAA1 and PNIPAM-AAm-*b*-PAA2, respectively.

Optical transmittance determined for PNIPAM-AAm-*b*-PAA1 and PNIPAM-AAm-*b*-PAA2 are shown as a function of temperature in Fig. 1. The optical transmittance of aqueous PNIPAM-AAm-*b*-PAA1 was almost unity at temperatures below 42.4 °C, and decreased rapidly with rising temperature between 42.4 and 43.1 °C, and vanished at higher temperatures. The sharpness of the transition was estimated from the temperature distance ΔT between 5% transmittance and 95% transmittance: ΔT was 0.7 K for PNIPAM-AAm-*b*-PAA1 and 0.9 K for PNIPAM-AAm-*b*-PAA2. T_{cp} was determined as 42.6 and 42.4 °C for PNIPAM-AAm-*b*-PAA1 and PNIPAM-AAm-

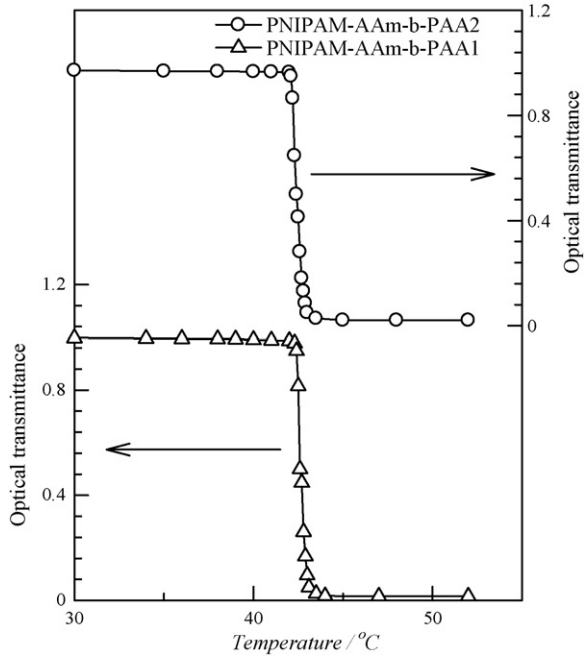

Fig. 1. Temperature dependence of optical transmittance of copolymers in water ($c = 5.00 \times 10^{-3}$ g cm^{-3}) for PNIPAM-AAm-*b*-PAA1 (△) and PNIPAM-AAm-*b*-PAA2 (◯).

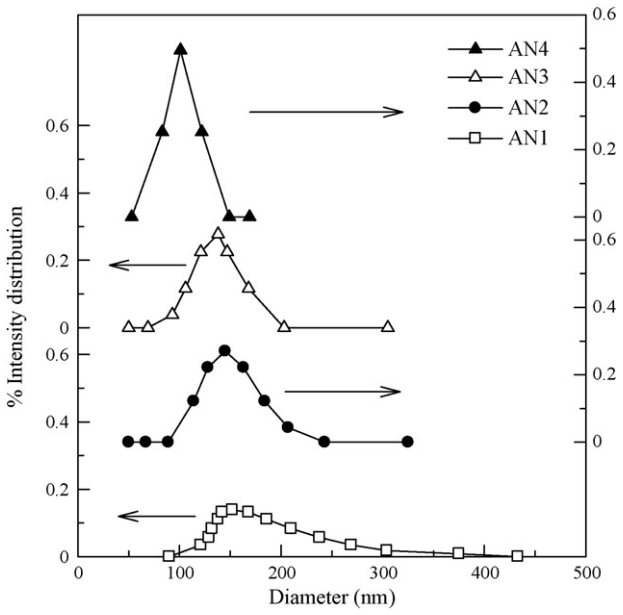

Fig. 2. Size distributions of albumin nanospheres measured by DLS: AN1 (□), AN2 (●), AN3 (△) and AN4 (▲).

b-PAA2 when the optical transmittance of the solutions crossed 50% as the temperature increased.

In a previous study, we have found that the reciprocals of T_{cp} of aqueous solution of PNIPAM-AAm increased linearly against volume fraction of NIPAM γ (determined from the volume ratio of NIPAM to the sum of NIPAM and AAm), where the slope was related to the interaction energy difference between the solvent-NIPAM and the solvent-AAm (Shen et al., 2006a). Therefore, T_{cp} of PNIPAM-AAm-*b*-PAA can also be controlled by γ. T_{cp} of PNIPAM-AAm-*b*-PAA1 and PNIPAM-AAm-*b*-PAA2, which can be decreased by decreasing the γ, are slightly higher than that of PNIPAM-AAm (41.0 °C) with the same γ. This was considered to result from hydration contribution from hydrophilic AA in the polymer.

The copolymers coherent to the current strategy need to change from hydrophilic type to hydrophobic type around 42 °C, and the change must be very sensitive to temperature change to increase the targeting ability. Here, both PNIPAM-AAm-*b*-PAA1 and PNIPAM-AAm-*b*-PAA2 can meet these conditions.

3.2. Size control and TEM observation of albumin nanospheres

There are three different preparation methods for AN, based on desolvation (Langer et al., 2003), coacervation (Lin et al., 2001), or emulsion formation (Muller et al., 1996). In this paper, we prepared AN based on emulsion formation because the size of AN prepared by desolvation and coacervation cannot be controlled easily. In order to obtain AN with diameter around 100 nm, which is required for intravenous administration, the effect of the output power of ultrasonic disruptor on the particle size and size distribution was investigated.

The preparation results of AN1, AN2, AN3 and AN4 are summarized in Table 1 and Fig. 2. The yield for each AN sample was between 80 and 88%. $\bar{d}$ and CV values both decreased as the output power of the ultrasonic disruptor increased, by which the particle size and size distribution of albumin nanospheres can be controlled. The appropriate output power of the ultrasonic disruptor was obtained (165 W, AN4 sample) according to the requirement of the size of AN in drug delivery.

Fig. 3(a–c) was TEM photo of AN4 observed at 49,000, 61,000 and 81,000 magnification, respectively. From these pictures, it was found that the albumin nanospheres were dispersed

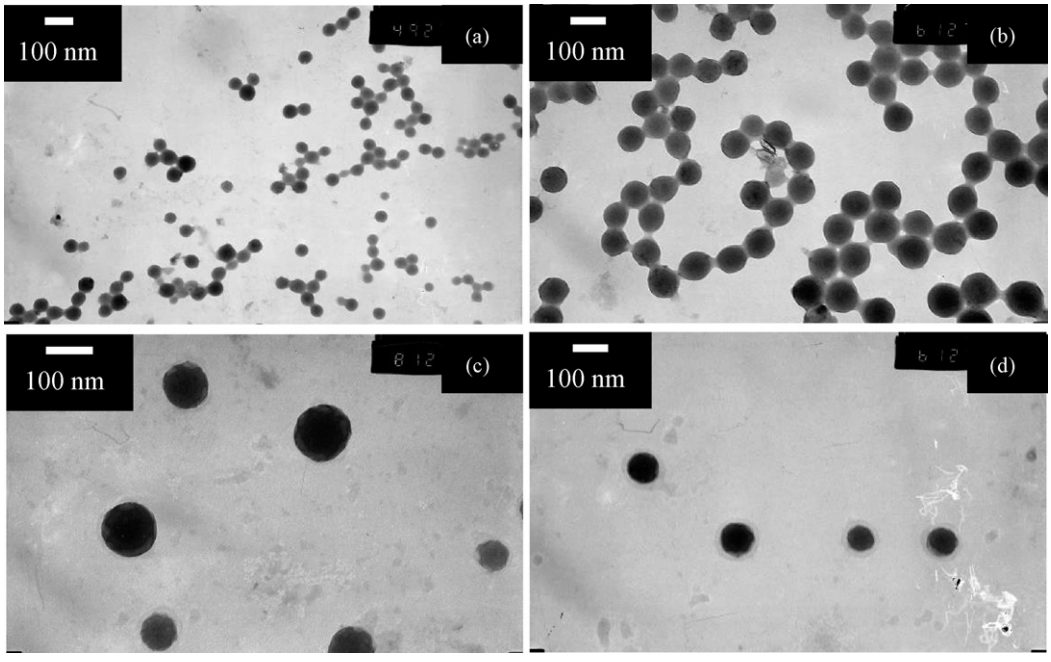

Fig. 3. TEM photo of AN4 observed at 49,000 magnification (a), 61,000 magnification (b) and 81,000 magnification (c) and PAN1 observed at 61,000 magnification (d).

well in pure water, the coalescence and aggregation of nanoparticles were almost not found, the particles were spherical in shape and the surfaces of the particles were smooth. From TEM pictures, the average diameter of AN4, smaller than the result of DLS (102 nm), was estimated to be below 100 nm due to the swelling of AN because TEM was observed at dry state of AN and DLS was determined at wet state of AN. Therefore, AN can be achieved as a long-circulating system with a size range below 200 nm in diameter for the current drug delivery scheme.

3.3. Optimization of nanosphere preparation by drug loading ratio and entrapment efficiency

The ability of AN to carry a model drug RB was evaluated. RB is a water-soluble reagent (M_w = 1017.6 Da) with a high ability of protein binding (Lillie, 1977) and widely used as a diagnostic agent due to its high extinction coefficient at 548 nm. In this paper, RB was used as a model drug, and the influence of the RB/BSA ratio, the emulsifier concentration in the oil phase and the concentration of glutaraldehyde on the drug loading ratio and the entrapment efficiency were investigated. The results of preparation of RB-loaded AN are summarized in Table 2. If not specified, the RB/BSA ratio, emulsifier concentration, glutaraldehyde concentration and output power of the ultrasonic disruptor were fixed at 2.50 μg RB/mg BSA, 6.0 wt.%, 0.85 mg GA/mg BSA and 165 W, respectively, in the following experiments.

There are three main factors which are considered to affect the drug loading ratio and entrapment efficiency of RB in albumin nanospheres: (1) the binding degree between the drug and the albumin molecule; (2) coalescence and break-up of emulsion droplets, leading to leakage of drug; (3) diffusion of drug from water phase to oil phase.

Fig. 4(a) shows the capacity of albumin nanospheres for RB loading as a function of the drug/initial albumin ratio (RB/BSA ratio). The high drug entrapment efficiency in AN was achieved, up to 83.0% at low RB/BSA ratio. With increasing the RB/BSA ratio, the drug loading ratio increased quickly at RB/BSA ratios lower than 2.50 μg RB/mg BSA, but increased slowly at RB/BSA ratios higher than 2.50 μg RB/mg BSA. However, the entrapment efficiency decreased gently at RB/BSA ratios lower than 2.50 μg RB/mg BSA, but decreased rapidly at higher than 2.50 μg RB/mg BSA. That was because the binding degree between RB and the albumin molecule increased with the increase of initial RB/BSA ratio, attain to maximum at a RB/BSA ratio and the RB leaked out easily when the binding sites of RB on the albumin molecules have been exhausted.

Fig. 4(b) shows the effect of oil-soluble emulsifier concentration on the drug loading ratio and entrapment efficiency. The drug loading ratio and the entrapment efficiency did not change apparently when Arlacel83 concentration was higher than 4 wt.%, but decreased with decrease of Arlacel83 concentration from 4 wt.%. Because oil-soluble emulsifier plays an important role in the maintenance of emulsion stability, the coalescence and break-up of the emulsion droplets can be avoided or retarded. Therefore, the drug entrapment efficiency usually

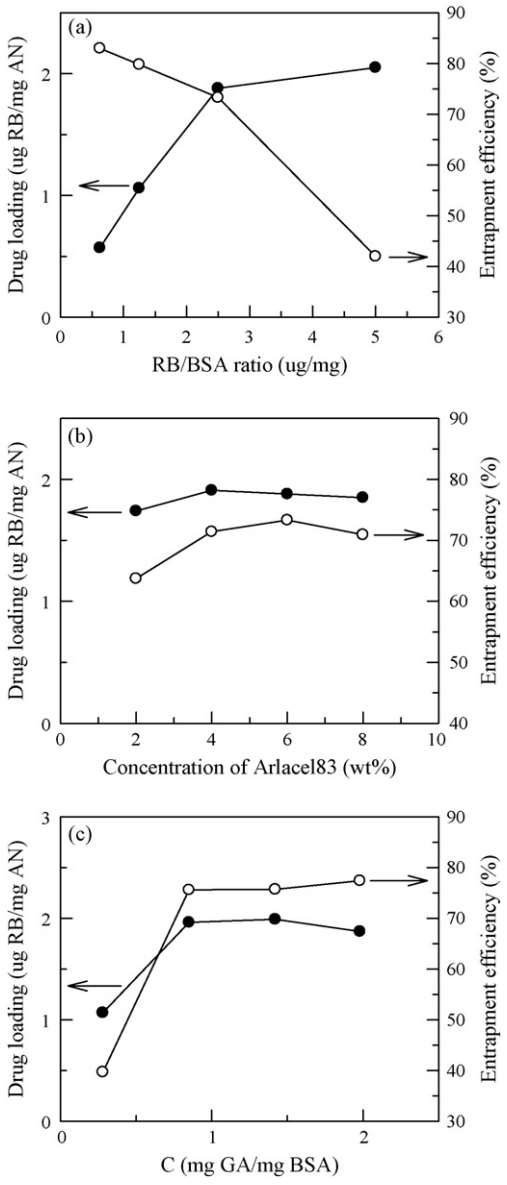

Fig. 4. Influence of RB/BSA ratio (a), emulsifier concentration in the oil phase (b) and concentration of glutaraldehyde (c) on the drug loading ratio (μg RB/mg AN) and the entrapment efficiency (expressed in %) in AN.

can be improved by increasing the concentration of emulsifier (Liu et al., 2005).

Although RB is a water-soluble drug, it also can be dissolved in cyclohexane appreciably. RB also may be released during the washing process by pure water or physiological saline. Therefore, the effect of the diffusion of RB from water phase to oil phase or the loss of RB during washing process on the drug loading ratio and entrapment efficiency is not neglectable. Fig. 4(c) shows the effect of glutaraldehyde concentration on the drug loading ratio and entrapment efficiency. The drug loading ratio and the entrapment efficiency decreased rapidly with decreasing the glutaraldehyde concentration from 0.85 mg GA/mg BSA. However, they were significantly close with various glutaraldehyde concentrations when it was higher than 0.85 mg GA/mg BSA. The AN with a higher cross-linking degree would be

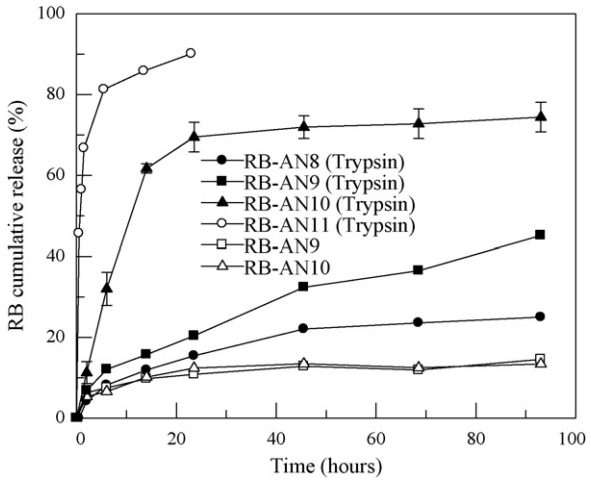

Fig. 5. RB release from RB-AN9 (□) and RB-AN10 (△) in pH 7.4 PBS at 37 °C and RB release from RB-AN8 (●), RB-AN9 (■), RB-AN10 (▲) and RB-AN11 (◯) in pH 7.4 PBS containing 0.20 mg/mL trypsin at 37 °C. Error bars represent calculations of standard error on the basis of triplicate determinations.

difficult to swell and break-up, and the RB would be difficult to be released. Consequently, the drug loading ratio and drug entrapment efficiency increased by increasing the amounts of glutaraldehyde and attained to a maximum value because most of the amino groups on the surface of the albumin nanospheres have reacted with glutaraldehyde.

3.4. RB release from albumin nanospheres

Fig. 5 shows that the release of RB from RB-AN9 and RB-AN10 in PBS (pH 7.4, 10 mM) at 37 °C was very slow and their release behavior was similar. After 93.0 h, only around 14.5 and 13.4% of loaded drug were released from RB-AN9 and RB-AN10, respectively. The release of RB from RB-AN8, RB-AN9, RB-AN10 and RB-AN11 in PBS (pH 7.4, 10 mM) containing 0.20 mg/mL of trypsin at 37 °C was also shown in Fig. 5. In the presence of trypsin, the release of RB from RB-AN9 and RB-AN10 were dramatically accelerated. The concentrations of glutaraldehyde were 1.98, 1.42, 0.85 and 0.28 mg GA/mg BSA for RB-AN8, RB-AN9, RB-AN10 and RB-AN11. After 2.0 h about 4.2, 6.8 and 11.2 ± 1.3% of loaded RB were released and after 93.0 h about 25.0, 45.1 and 74.4 ± 3.7% were released from RB-AN8, RB-AN9 and RB-AN10, respectively. The RB release from RB-AN11 was fast, after 0.5 h about 45.6% and after 23 h about 90.1% of loaded RB was released. Therefore, it can be concluded that release rate of RB from albumin nanospheres increased with decrease of glutaraldehyde amount.

For the purpose of using the albumin nanospheres as anti-cancer drug carrier for tumor targeting, the slower the drug release from the particles while during circulation in the blood stream after intravenous injection, the weaker the side-effect of the anti-cancer drugs, and release rate should increase at the target sites (cancer cells or cancer tissues) which contain more enzymes than the blood (Muller et al., 1996). The fact that the release of RB from the albumin nanospheres in pH 7.4 PBS at 37 °C in the absence of the proteinase trypsin was very slow and dramatically increased in the presence of trypsin indicates that the AN can be used as an anti-cancer drug carrier.

3.5. Preparation result of PNIPAM-AAm-b-PAA-conjugated albumin nanospheres

We have tried to conjugate poly(*N*-isopropylacrylamide-*co*-acrylamide)-*block*-polyacrylic acid (PNIPAM-AAm-*b*-PAAc) onto the surface of AN using the carboxyl groups of the polymers to react with the amino groups of the AN (Shen et al., 2006b). However, the cross-linker glutaraldehyde had consumed most of amino groups during the cross-linking process, so that PNIPAM-AAm-*b*-PAAc cannot be conjugated on AN successfully. Therefore, here we used PNIPAM-AAm-*b*-PAA with several amino groups at the end of the polymer chains, which can react with the carboxyl groups on the surface of AN.

The results of preparation of RB-PAN are summarized in Table 2. The drug loading ratio of RB-PAN1 and RB-PAN2 were 1.08 and 0.91 μg RB/mg AN, and the entrapment efficiencies were 39.3 and 36.1%, respectively. The low entrapment efficiencies were considered due to the loss during the conjugation process.

Furthermore, the amounts of PNIPAM-AAm-*b*-PAA1 and PNIPAM-AAm-*b*-PAA2 on the surface of AN were determined to be 0.68 and 0.75 nmol/mg AN for PAN1 and PAN2, respectively.

Approximating

$$\frac{4}{3}\pi\left(\frac{\bar{d}}{2}\right)^3 \cong n \times \frac{4}{3}\pi\left(\frac{d_0}{2}\right)^3 \quad (3)$$

where d_0 is the mean diameter of BSA, and n is the amount of BSA molecular in one nanosphere. d_0 was determined to be 5.1 ± 0.1 nm by DLS at room temperature with the concentration of 5.0 mg/mL. From Eq. (3), we can obtain that $n \cong 8000$ because of $\bar{d} = 102$ nm. So that, we can calculate that the amount of AN is 1.894×10^{-9} mol within 1.0 g AN (approximating that 1.0 g AN was consisted of 1.0 g BSA). Therefore, the amounts of PNIPAM-AAm-*b*-PAA1 and PNIPAM-AAm-*b*-PAA2 on the surface of AN were calculated to be 359 and 396 mol/mol AN, respectively.

3.6. Hydrodynamic diameter of PNIPAM-AAm-b-PAA-conjugated albumin nanospheres

The D_h of PAN1 and PAN2 were 142.9 and 157.0 nm, respectively at 38.4 °C and decreased, respectively to 128.4 and 145.4 nm at 43.5 °C, as shown in Fig. 6. The D_h of PAN decreased with increasing temperature because of the change in comformation of PNIPAM-AAm-*b*-PAA chains from the random coil to compact globule, which indicated the fine temperature sensitivity of PAN prepared in this study.

The size distributions of PAN1 and PAN2 at room temperature were shown in Fig. 7. It is clear that the size distributions of PAN1 and PAN2 became broader than AN4 (shown in Fig. 2) due to the molecular weight distributions of PNIPAM-AAm-*b*-PAA1 and PNIPAM-AAm-*b*-PAA2. The CV values of AN4, PAN1 and

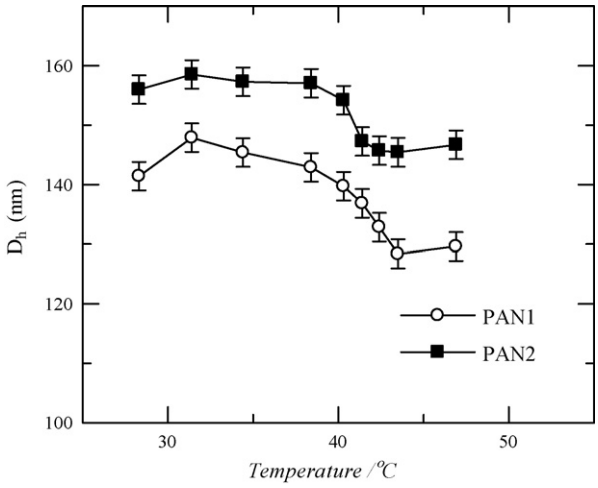

Fig. 6. Temperature dependence of D_h of PNIPAM-AAm-*b*-PAA-conjugated albumin nanospheres in water for PAN1 (◯) and PAN2 (■).

PAN2 were 0.140, 0.226 and 0.234, respectively. From Fig. 3(d), it is obvious that the morphology of PAN1 was similar to that of AN4 because the PNIPAM-AAm-AA1 on the surface of AN was too slender to be visible.

3.7. RB release from PNIPAM-AAm-b-PAA-conjugated albumin nanospheres

After 8.0 h, 41% of RB was released from RB-AN10 at 37 ± 1 °C. Therefore, the drug loading ratio of RB-AN12 (renamed sample of RN-AN10 after 8.0 h of drug release) was calculated to be 1.06 μg RB/mg AN, which was close to the drug loading ratio of RB-PAN1 and RB-PAN2.

Fig. 8 shows the RB release from RB-AN12, RB-PAN1 and RB-PAN2 at 37 °C and from RB-PAN1 and RB-PAN2 at 43 °C in pH 7.4 PBS containing 0.20 mg/mL trypsin. The results showed that the RB release from RB-AN12 was faster than from RB-PAN1 and RB-PAN2 at 37 °C, and that from RB-PAN2 was slowest. Moreover, the RB release from RB-PAN1 was also faster than from RN-PAN2 at 43 °C. After 14.0 h about 46.7 and 39.1% of loaded RB were released and after 93.0 h about 65.5 and 53.8% were released from RB-PAN1 and RB-PAN2 at

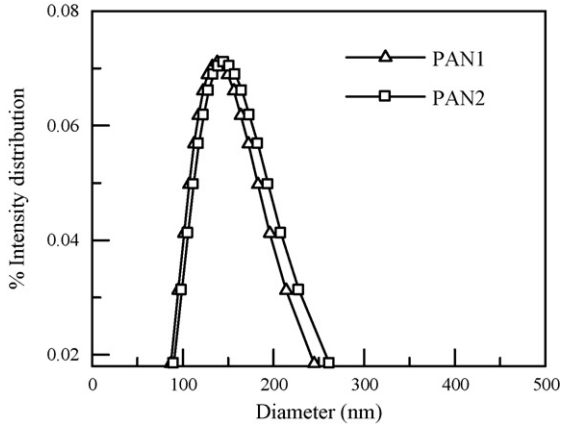

Fig. 7. Size distributions of PAN1 (△) and PAN2 (□).

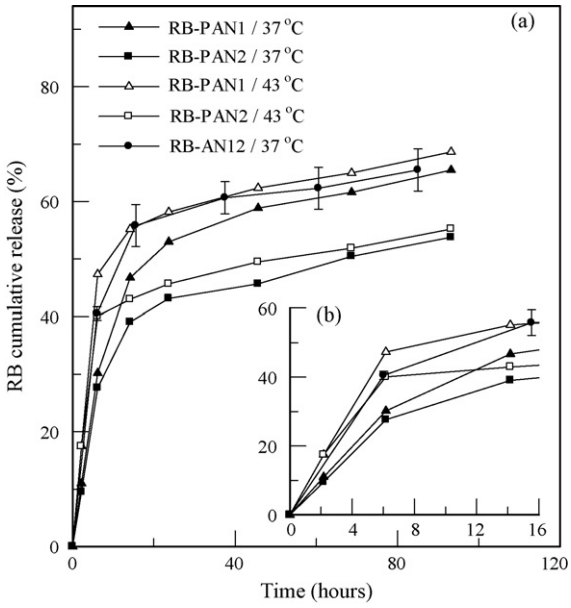

Fig. 8. RB release from RB-AN12 (●), RB-PAN1 (▲) and RB-PAN2 (■) in pH 7.4 PBS containing 0.20 mg/mL trypsin at 37 °C, and RB release from RB-PAN1 (△) and RB-PAN2 (□) in pH 7.4 PBS containing 0.20 mg/mL trypsin at 43 °C within 93 h (a). The RB release behavior within 16 h (b). Error bars represent calculations of standard error on the basis of triplicate determinations.

37 °C, respectively. After 6.0 h about 40.5% of loaded RB was released and after 85.0 h about 65.5% was released from RB-AN12 at 37 °C. After 14.0 h about 55.2 and 43.0% of loaded RB were released and after 93.0 h about 68.6 and 55.2% were released from RB-PAN1 and RB-PAN2 at 43 °C, respectively. The RB release from both RB-PAN1 and RB-PAN2 are faster at 43 °C than at 37 °C.

The release of RB from RB-PAN compared with RB-AN in the presence of the enzyme was slower and the release rate of RB from RB-PAN decreased with increasing the molecular weight of PNIPAM-AAm-*b*-PAA, which suggested that the existence of a steric hydrophilic barrier on the surface of the AN made digestion of the AN more difficult. Moreover, the release of RB from RB-PAN at the temperature above T_{cp} of PNIPAM-AAm-*b*-PAA was faster than that below the T_{cp}. That was because temperature-responsive polymers on the surface of RB-PAN were not so dense and the interspace between the temperature-responsive polymer chains increased after they shrunk due to the high temperature (as shown in Scheme 1b), so that the biodegradable albumin nanospheres were attacked and degraded easily by trypsin and the drug release rate from the PAN increased.

These results indicated that PAN can circulate in blood stream after intravenous injection with a longer half-life and less drug release, and release the drug fast after accumulated in tumor cells. It can overcome the disadvantages of temperature-responsive polymeric micelles, the instability because of being constructed by hydrophobic interaction and the decreasing drug release rate from the micelles after accumulated in tumor cells. Animal experiments are being carried out to prove the advantage of this new drug carrier.

4. Conclusions

Novel thermal targeting anti-cancer drug carrier PAN was developed by conjugating PNIPAM-AAm-*b*-PAA on the surface of AN. DLS measurement showed that PAN was temperature sensitive, which indicated that they can selectively accumulate in solid tumors that are maintained above physiological temperature due to local hyperthermia. 'In vitro' release studies proved the slow drug release from AN in the absence of the proteinase and dramatic increase in the presence of proteinase, and fast drug release from PAN at the temperature above T_{cp} of PNIPAM-AAm-*b*-PAA, which indicated the slow drug release from PAN while circulating in the blood stream after intravenous injection and the increase of drug release rate at the target sites (cancer cells or cancer tissues). The release of drug from PAN at the temperature above T_{cp} of PNIPAM-AAm-*b*-PAA was faster than that at the temperature blow the T_{cp}, which implied that PAN overcame the disadvantage of temperature-responsive polymeric micelles. From these results, it is expected that PAN can be used as thermal targeting anti-cancer drug carrier and eliminate undesirable side effects generated by free drugs for cancerous chemotherapy.

Acknowledgements

The authors thank the Ministry of Education, Culture, Sports, Sciences, and Technology of Japan for providing scholarship to the first author to pursue his research at the Department of Biological and Chemical Engineering, Faculty of Engineering, Gunma University. Financial support from the National Nature Science Foundation of China (contract nos. 20536050, 20221603 and 20376082) is gratefully acknowledged.

References

Brigger, I., Dubernet, C., Couvreur, P., 2002. Nanoparticles in cancer therapy and diagnosis. Adv. Drug. Deliv. Rev. 54, 631–651.

Chung, J.E., Yokoyama, M., Okano, T., 2000. Inner core segment design for drug delivery control of thermo-responsive polymeric micelles. J. Controlled Release 65, 93–103.

Gong, L.S., Zhang, Y.D., Liu, S., 2004. Target distribution of magnetic albumin nanoparticles containing adriamycin in transplanted rat liver cancer model. Hepatobiliary Pancreat. Dis. Int. 3, 365–368.

Illum, L., Davis, S.S., 1984. The organ uptake of intravenously administered colloidal particles can be altered using a non-ionic surfactant (Poloxamer 338). FEBS Lett. 167, 79–82.

Inoue, T., Chen, G., Nakamae, K., Hoffman, A.S., 1998. An AB block copolymer of oligo(methyl methacrylate) and poly(acrylic acid) for micellar delivery of hydrophobic drugs. J. Controlled Release 51, 221–229.

Isojima, T., Fujii, S., Kubota, K., Hamano, K., 1999. Near-critical dynamical behavior of an ionic micellar solution. J. Chem. Phys. 111, 9839–9846.

Jeong, J.H., Kim, S.W., Park, T.G., 2003. A new antisense oligonucleotide delivery system based on self-assembled ODN-PEG hybrid conjugate micelles. J. Controlled Release 93, 183–191.

Kohori, F., Sakai, K., Aoyagi, T., Yokoyama, M., Yamato, M., Sakurai, Y., Okano, T., 1999. Control of adriamycin cytotoxic activity using thermally responsive polymeric micelles composed of poly(*N*-isopropylacrylamide-*co*-*N*,*N*-dimethylacrylamide)-b-poly($_{D,L}$-lactide). Colloids Surf. B: Biointerfaces 16, 195–205.

Kwon, G.S., Naito, M., Yokoyama, M., Okano, T., Sakurai, Y., Kataoka, K., 1995. Physical entrapment of adriamycin in AB block copolymer micelles. Pharm. Res. 12, 192–195.

Langer, K., Balthasar, S., Vogel, V., Dinauer, N., Briesen, H.V., Schubert, D., 2003. Optimization of the preparation process for human serum albumin (HSA) nanoparticles. Int. J. Pharm. 257, 169–180.

Lillie, R.D., 1977. In: H.J. Conn's Biological Stains, 9th ed., Williams & Wilkins Company, Baltimore, MD, pp. 350–351.

Lin, W., Garnett, M.C., Schacht, E., Davis, S.S., Illum, L., 1999. Preparation and in vitro characterization of HSA-mPEG nanoparticles. Int. J. Pharm. 189, 161–170.

Lin, W., Garnett, M.C., Davis, S.S., Schacht, E., Ferruti, P., Illum, L., 2001. Preparation and characterisation of rose Bengal-loaded surface-modified albumin nanoparticles. J. Controlled Release 71, 117–126.

Liu, R., Ma, G.H., Meng, F.T., Su, Z.G., 2005. Preparation of uniform-sized PLA microcapsules by combining Shirasu Porous Glass membrane emulsification technique and multiple emulsion-solvent evaporation method. J. Controlled Release 103, 31–43.

Moghimi, S.M., Muir, I.S., Illum, L., Davis, S.S., Bachofen, V.K., 1993. Coating particles with a block co-polymer (poloxamine-908) suppresses opsonization but permits the activity of dysopsonins in the serum. Biochim. Biophys. Acta 1179, 157–165.

Moghimi, S.M., Hunter, A.C., Murray, J.C., 2001. Long-circulating and target-specific nanoparticles: theory to practice. Pharmacol. Rev. 53, 283–318.

Muller, B.G., Leuenberger, H., Kissel, T., 1996. Albumin nanospheres as carriers for passive drug targeting: an optimized manufacturing technique. Pharm. Res. 13, 32–37.

Ohya, S., Nakayama, Y., Matsuda, T., 2004. In vivo evaluation of poly(*N*-isopropylacrylamide) (PNIPAM)-grafted gelatin as an in situ-formable scaffold. J. Artif. Organs 7, 181–186.

Sheng, J., Samten, B.K., Xie, S.S., Wei, S.L., 1995. Study on the specific killing activity of albumin nanoparticles containing adriamycin targeted by monoclonal antibody BDI-1 to human bladder cancer cells. Acta Pharm. Sin. 30, 706–710.

Sheng, X.Z., Liu, Z.Q., Wu, L.B., Tang, J., Zhao, C.R., Kong, L.B., Wang, Q., Wang, C.D., 2006. Technical feasibility and histopathologic studies of poly(*N*-isopropylacrylamide) as a non-adhesive embolic agent in swine rete mirabile. Chin. Med. J. 119, 391–396.

Shen, Z.Y., Terao, K., Maki, Y., Dobashi, T., Ma, G.H., Yamamoto, T., 2006a. Synthesis and phase behavior of aqueous poly(*N*-isopropylacrylamide-*co*-acrylamide), poly(*N*-iso- propyl acrylamide-*co*-*N*, *N*-dimethylacrylamide) and poly (*N*-isopropylacrylamide-*co*-2- hydroxyethyl methacrylate). Colloid Polym. Sci. 284, 1001–1007.

Shen, Z.Y., Ma, G.H., Dobashi, T., Maki, Y., Yoneyama, M., Yamamoto, T., 2006b. Synthesis and phase behavior of aqueous poly(*N*-isopropylacrylamide-*co*-acrylamide-*co*-acrylic acid). Trans. Mater. Res. Soc. Jpn. 31, 799–802.

Topp, M.D.C., Dijkstra, P.J., Talsma, H., Feijen, J., 1997. Thermosensitive micelle-forming block copolymers of poly(ethylene glycol) and poly(*N*-isopropylacrylamide). Macromolecules 30, 8518–8520.

Yuan, F., 1998. Transvascular drug delivery in solid tumors. Semin. Radiat. Oncol. 8, 164–175.

Zhang, L., Hou, S., Mao, S., Wei, D., Song, X., Lu, Y., 2004. Uptake of folate-conjugated albumin nanoparticles to the SKOV3 cells. Int. J. Pharm. 287, 155–162.